International Journal of Heat and Mass Transfer 52 (2009) 716–723

Contents lists available at ScienceDirect

International Journal of Heat and Mass Transfer

journal homepage: www.elsevier.com/locate/ijhmt

Theoretical model for fast bubble growth in small channels with reference to startup of capillary pumped loops used in spacecraft thermal management systems

Tim J. LaClair, Issam Mudawar *

Boiling and Two-Phase Flow Laboratory (BTPFL), Purdue University International Electronic Cooling Alliance (PUIECA), 1288 Mechanical Engineering Bld., 585 Purdue Mall, West Lafayette, IN 47907, USA

ARTICLE INFO

Article history:
Received 31 December 2007
Received in revised form 11 July 2008
Available online 12 September 2008

ABSTRACT

A capillary pumped loop (CPL) is a closed two-phase loop in which capillary forces developed in a wicked evaporator passively pump the working fluid over long distances to dissipate heat from electronic and power sources. Because it has no moving parts and requires minimal power to sustain operation, the CPL is considered an enabling technology for thermal management of spacecraft. While the steady-state operation of a CPL is fairly well understood, its thermal response during startup remains very illusive. During the startup, initial vapor bubble growth in the evaporator is responsible for liquid acceleration that results in a differential pressure spike. A large pressure spike can deprime the evaporator by forcing vapor into the evaporator's liquid-saturated wick, which is the only failure mode of a CPL other than fluid loss or physical damage to the loop. In this study, a numerical transient 3D model is constructed to predict the initial bubble growth. This model is used to examine the influence of initial system superheat, evaporator groove shape and size, and wick material. A simplified model is also presented which facilitates the assessment of parametric influences by analytic means. It is shown how these design parameters may be optimized to greatly reduce the bubble growth rate and therefore help prevent a deprime.

1. Introduction

1.1. Thermal management challenges of spacecraft

Two-phase cooling systems have been widely examined for thermal management of electronic devices in terrestrial applications. By capitalizing upon the merits of latent heat exchange, the performance of these systems is far superior to those of their single-phase counterparts. Another key advantage of a two-phase cooling system is the ability to tackle appreciable variations in the dissipated heat flux corresponding to only mild changes in the device temperature [1].

Spacecraft pose very unique challenges that are mostly the result of operating environment, which influences every aspect of the heat acquisition, transport and rejection. Waste heat from the electronic assemblies is transported to radiator panels that reject the heat by radiation to deep space. Long distances between the electronic assemblies and radiator panels preclude the use of conventional heat pipes. Mechanical pumps, which are essential to most two-phase cooling loops, are also undesirable in spacecraft because they can consume a significant fraction of a spacecraft's limited "power budget." Furthermore, spacecraft are designed for 10 years or more of maintenance-free operation, precluding the use of moving parts that are prone to mechanical failure.

1.2. Spacecraft thermal management using capillary pumped loops

Capillary pumped loops (CPLs) are two-phase systems designed to transport heat over a length of up to tens of meters for heat rejection from one or multiple heat sources. A CPL is a closed fluid loop in which capillary forces developed in a wicked evaporator passively pump the working fluid through the rest of the loop with no energy required other than the heat that the loop acquires and rejects. Fig. 1 shows a schematic of a basic CPL. Heat from the electronic sources is conducted through a metal flange to the outer wall of the CPL's evaporator. During normal operation, the working fluid enters the evaporator in liquid state, where it extracts the waste heat by evaporation. The fluid exits the evaporator in vapor state and flows to the condenser (which is attached to radiator panels) where it is converted back to liquid state. A reservoir is used to maintain excess fluid inventory for the CPL and may be thermally controlled to set the loop's saturation temperature and pressure.

The evaporator is by far the most critical component of the CPL because it provides the pressure rise necessary to pump the fluid throughout the loop. In its most basic form, the evaporator consists of a grooved cylindrical metal shell that encases a porous, annular wick as illustrated in Fig. 2. The incoming liquid fills the center of

* Corresponding author. Tel.: +1 765 494 5705; fax: +1 765 494 0539.
E-mail address: mudawar@ecn.purdue.edu (I. Mudawar).

0017-9310/$ - see front matter © 2008 Elsevier Ltd. All rights reserved.
doi:10.1016/j.ijheatmasstransfer.2008.07.010

Nomenclature

A	area
A_{gr}	cross-sectional area of groove
c	parameter defined in Eq. (13b)
c_p	specific heat
D_h	hydraulic diameter of groove
$f_i(\vec{r})$	initial temperature distribution function
h_{fg}	latent heat of vaporization
k	thermal conductivity
k_G	geometric mean thermal conductivity
L_0	initial vapor length in groove
P	pressure
P_{gr}	perimeter of groove's cross-section
P_w	wetted perimeter of groove in contact with liquid-saturated wick
$q''(z,t)$	heat flux into vapor-filled portion of groove in analytical model
$q''_{gr}(\vec{r},t)$	heat flux into vapor-filled portion of groove
$q''_s(t)$	surface heat flux for conduction from semi-infinite medium
$\vec{r}$	position vector
t	time
T	temperature
T_{sat}	saturation temperature
ΔT_{sh}	initial evaporator superheat
$\dot{V}_g(t)$	volumetric growth rate of vapor in groove
z	axial coordinate
$z_g(t)$	vapor length in 3D model
$\dot{z}_g(t)$	axial vapor growth rate in 3D model
$Z_g(t)$	vapor length in simplified analytical model
$\dot{Z}_g(t)$	axial vapor growth rate in simplified analytical model
$Z_g^{-1}(z)$	inverse function of $Z_g(t)$

Greek symbols

α	thermal diffusivity
Γ_1	interface between metal wall and vapor-filled portion of groove
Γ_2	interface between wick and vapor-filled portion of groove
ρ	density
ρ_g	density of saturated vapor
φ	wick porosity

Subscripts

f	liquid in wick voids
i	evaporator subdomains defined in Fig. 5 (i = 1–4)
s	solid material of wick
sat	saturation

the evaporator, and is drawn radially outwards through the wick. The liquid evaporates at the wick's boundary in the grooves of the metal wall, where menisci are formed. The capillary pressure rise across these menisci is responsible for circulating the fluid throughout the CPL. The metal wall's grooves serve as vapor flow passages for the evaporator.

Several attributes render the CPL an enabling technology for thermal management of spacecraft [2,3]. These include requiring minimal external power to sustain operation, ability to passively transfer the heat over long distances while incurring negligible temperature changes, very low vibration levels, general simplicity, and, in the absence of moving parts, the potential for long life [2–5]. While some terrestrial applications may someday utilize CPLs, the presence of a gravity field can adversely affect thermal performance; hence, CPLs are better suited for space operation.

1.3. CPL startup concerns

Reliable operation of a CPL in the manner described in the previous section requires that only liquid be present in the liquid transport line and reservoir line, and in the evaporator core and wick. This ensures continuous liquid supply to the wick–groove boundary where evaporation takes place. Any vapor or gas bubbles in the "liquid side" of a CPL may eventually result in a *deprime*, which is ultimately the only failure mode of a CPL other than fluid loss or physical damage to the loop. The presence of non-condensible gases poses serious startup challenges [5–7]. Here, evaporation into a bubble containing non-condensible gases can occur at a temperature below the pure fluid's saturation temperature corresponding to the system pressure [8]. These non-condensible gas issues are beyond the scope of the present study.

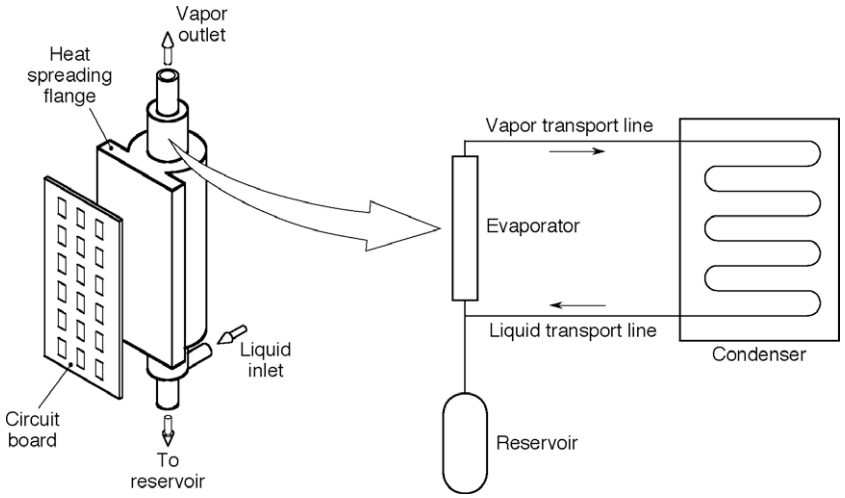

Fig. 1. Basic CPL configuration and circuit board attachment to tubular CPL evaporator.

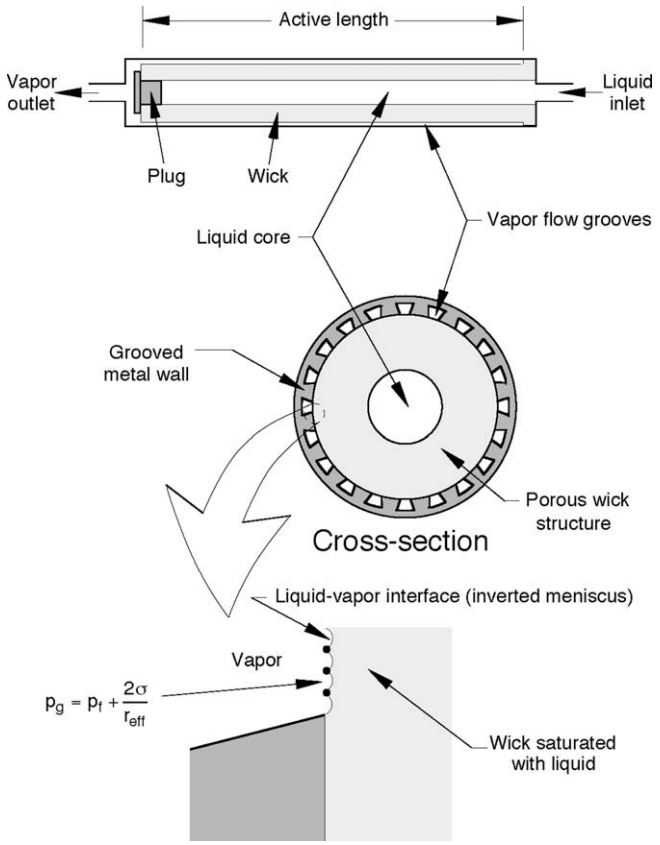

Fig. 2. Evaporator construction and groove detail showing liquid–vapor menisci at wick–groove interface.

Following pressure priming but before the CPL can begin its steady-state mode of operation, a *startup* procedure must be carried out. The purpose of this startup procedure, which is inherently transient in nature, is to bridge the gap between the pressure priming phase and the normal steady-state mode of operation. The following is a summary of all these phases of CPL operation:

(1) *Pressure priming*: the entire CPL is pressurized while all of the working fluid is stagnant and, other than in the reservoir, is in liquid phase.
(2) *Startup*: the liquid is cleared from the vapor lines of the CPL without allowing vapor to be transported to, or formed inside of, the liquid side of the loop.
(3) *Normal operation*: vapor fills approximately half the length of the loop as illustrated in Fig. 1, and the working fluid flows steadily through the loop.

In spite of continued research and many design developments made since the introduction of the CPL, startup is too frequently unsuccessful. Difficulty with startup has, arguably, been the single greatest factor limiting the wide acceptance of CPLs for thermal management of spacecraft. Startup failures and other system anomalies that can be attributed to incomplete or improper priming have plagued flight experiments [9–12]. Recently, the CPL-based thermal control system that was designed for the Mars Polar Lander (MPL) of the Mars'98 mission [13] was eliminated from the spacecraft due to the CPL's inability to reliably start during system level testing.

The present study concerns only the startup phase of a CPL that has already been pressure-primed.

1.4. Study objectives

Surprisingly, very little theoretical work has been performed that addresses the fundamental issues of CPL startup. Improved understanding and better predictive tools for fluid flow, pressure, and thermal transients during the startup may enable new evaporator and system designs that allow for faster and more reliable CPL operation.

The present paper concerns the key fluid flow and heat transfer problem associated with the startup: *initial vapor growth* within the evaporator's grooves. A very fast initial vapor growth can lead to a *pressure spike* in the evaporator grooves, tending to force vapor from the grooves back through the wick, effectively interrupting the liquid supply, and initiating a deprime. Aside from a detailed model of the vapor growth, a simplified model is developed that enables the assessment of the dependence of initial vapor growth on the CPL's various design parameters using analytic means. Based on results of both the detailed and simplified models, design recommendations are presented that have the potential to decrease the initial vapor growth rate and, hence, the pressure spike.

2. Vapor growth model

2.1. Bubble growth in small channels

Vapor formation and growth in small heated channels is fundamentally different from that in large channels. Classical descriptions of the latter point to nucleation of a number of bubbles that grow, depart, and coalesce with one another, resulting in a several possible flow regimes, bubbly, slug, churn, and annular. However, in small channels, a nucleating bubble can quickly grow to engulf the entire cross-sectional, and as the heat flux is increased, a slug flow pattern evolves as the initial bubble grows axially by evaporation [14,15]. Fig. 3 illustrates the drastic differences between the two extreme boiling situations.

As will be explained later, vapor formation and growth in the grooves of a CPL are far more complicated than in a simple heated small channel. However, the growth of a nucleating bubble to the channel dimensions should be very fast for both situations. This observation will be used later in the model development.

2.2. Model rationale

The primary rationale for the proposed vapor growth model is as follows. It is postulated that, after a bubble nucleates in one of the CPL's evaporator grooves, subsequent vapor growth will be sustained by evaporation into the initial bubble. During this vapor growth phase, liquid previously occupying the groove from the pressure priming phase is displaced out of the evaporator through the vapor transport line and/or backwards through the wick; all of the excess liquid ultimately flows to the reservoir. The liquid flow raises the pressure and, hence, the saturation temperature in the evaporator, *which makes nucleation at other locations of the same*

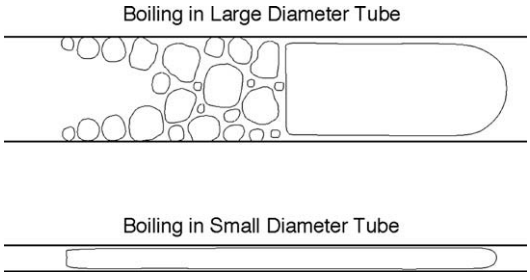

Fig. 3. Differences in boiling pattern between large and small diameter tubes.

groove or in other grooves unlikely during this initial vapor growth phase.

This process results in nucleation of a single bubble in only one evaporator groove followed by axial growth of the bubble along the same groove. After the first groove completely clears the liquid, the vapor begins to flow into neighboring grooves and the growth continues. Nucleation in the first groove occurs while liquid is stagnant in the evaporator, and the ensuing liquid acceleration in the first groove is greater than during any other period of the startup. Liquid flow through the wick during this period results in a differential pressure "spike" across the evaporator that is frequently observed immediately following boiling incipience in a CPL [2,3]. The magnitude of the pressure spike determines whether or not *vapor* will be injected through the wick and is, therefore, of paramount importance to the startup success.

After the nucleating bubble grows to a size where the groove's cross-section is filled with vapor, the metal wall dry outs very rapidly, leaving no liquid at the wall to evaporate. However, the wick, filled with superheated liquid, provides a constant supply of liquid to the groove to sustain the bubble growth by evaporation at the wick–groove boundary. As the volume of vapor increases along the groove, a larger area of the wick opens up to the saturated vapor in the groove, increasing the heat transfer rate, and *accelerating the vapor growth*. Although the metal wall represents the hottest region in the vicinity of the vapor, heat transfer from the wall directly to the vapor is small – the evaporative heat transfer coefficient across the wick–groove boundary is orders of magnitude greater than that due to conduction or convection to the vapor. However, as shown in Fig. 4, heat from the metal wall is conducted through the wick towards the wick–groove interface where the evaporation takes place.

When the first bubble forms in the evaporator, the metal wall is superheated above the saturation temperature. Also, at least part of, or perhaps the entire wick, is superheated [2]. Vapor growth occurs very rapidly along the groove as the superheat available in the evaporator is consumed by transient conduction towards the wick–groove interface, which is maintained at saturation temperature. In other words, much of the *initial vapor growth* is the result of relaxation of the initial superheat, rather than due to the externally supplied heat. The superheat of any additional thermal mass attached to the evaporator would simply accelerate the vapor growth.

2.3. Mathematical formulation of the transient 3D model

Based on the above rationale, a mathematical model of heat transfer in the evaporator following the initial bubble formation is developed. The equations governing axial vapor growth along the groove are based on heat conduction through the evaporator. Fig. 5 shows the notation for the various subdomains and interfaces used in the model for two popular evaporator designs. The first utilizes trapezoidal grooves that are extruded into the metal wall, while the second uses V-shaped grooves that are formed in the wick itself. With the exception of the vapor grooves, heat transfer in the evaporator is quite straightforward, governed by transient three-dimensional heat diffusion. Heat diffusion in the stagnant liquid core, the liquid-saturated wick, the metal wall, and in all groove regions filled with liquid, follows the heat diffusion equation:

$$(\rho c_p)_i \frac{\partial T_i}{\partial t} = \nabla \cdot (k_i \nabla T_i) \quad \text{for} \quad i = 1-4, \tag{1}$$

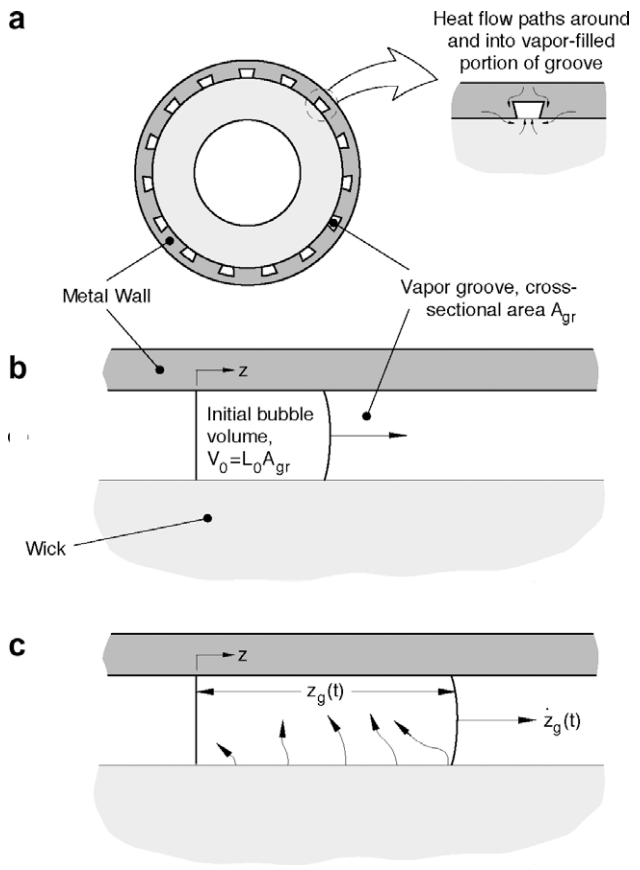

Fig. 4. Assumptions and geometry used in bubble growth model. (a) Evaporator cross-section. (b) Axial section of vapor groove at $t = 0$. (c) Axial section for $t > 0$. Because of transient conduction, heat flows non-uniformly through the wick and liquid evaporates rapidly into the bubble.

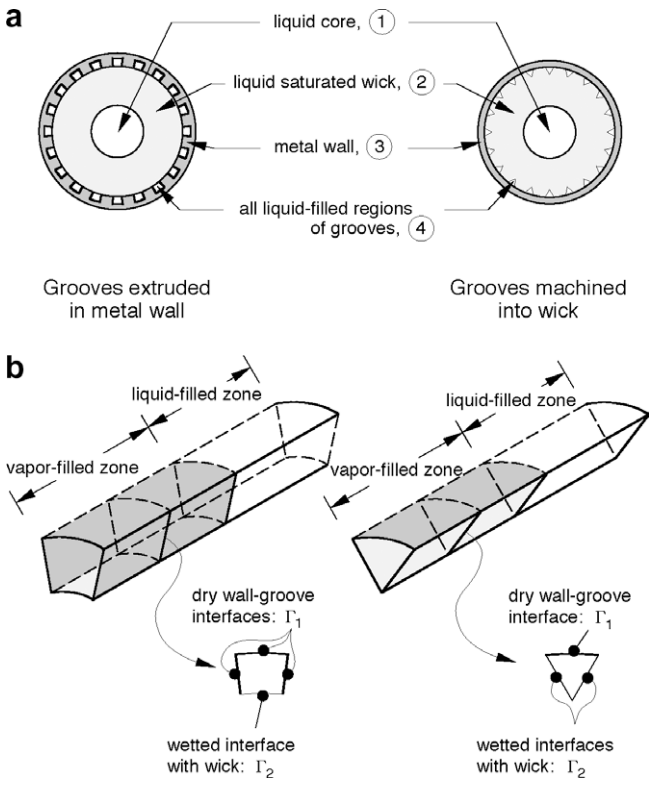

Fig. 5. Model domain and boundary conditions for extruded groove and groove-in-wick designs: (a) subdomain notation; (b) boundary condition interfaces for vapor-filled portion of groove.

where subscript i refers to the subdomains defined in Fig. 5. For all boundaries between the subdomains, continuities of temperature and heat flux are assumed. The liquid-saturated wick is treated as a homogenous material whose thermal conductivity is given by [16]

$$k_2 = k_G = k_s^{1-\varphi} k_f^{\varphi}, \tag{2}$$

where k_G, k_s, and k_f are the geometric mean conductivity of the porous medium, the conductivity of the solid, and the conductivity of the liquid, respectively, and φ is the porosity (void fraction) of the wick. The density-specific heat product of the wick is expressed as [16]

$$(\rho c_p)_2 = (1-\varphi)(\rho c_p)_s + \varphi(\rho c_p)_f, \tag{3}$$

where the subscripts s and f refer to the solid and liquid, respectively.

Boundaries in contact with the vapor require special consideration. For the metal wall adjacent to the vapor-filled portions of a groove (see Fig. 5), heat transfer to the vapor is neglected by assuming an adiabatic boundary condition:

$$\left.\frac{\partial T_3}{\partial n}\right|_{\Gamma_1} = 0, \tag{4}$$

where n is normal to the groove's wall boundary.

The increase in saturation temperature associated with the capillary pressure rise across the wick is quite small compared to the temperature superheat that is typically present in the evaporator to initiate startup. Since calculations made without including this change in saturation temperature actually provide conservative estimates of the pressure spike, this temperature change is excluded from the present analysis. Therefore, the evaporator's pressure is assumed uniform, and the boundary condition between the wick and the vapor-filled portion of the groove is expressed as

$$T_2|_{\Gamma_2} = T_{sat}(P_1). \tag{5}$$

In Fig. 5, the axial length of interfaces Γ_1 and Γ_2, denoted as $z_g(t)$, is time-dependent. The total rate of heat flow to the interface where evaporation occurs is obtained by integrating the heat flux over the wick–groove boundary for the portion of the groove that is filled with vapor. The vapor growth rate at time t is obtained from an energy balance at interface Γ_2:

$$\dot{z}_g(t) = \frac{1}{A_{gr}} \int_{\Gamma_2} \frac{q''_{gr}(\vec{r},t)}{\rho_g h_{fg}} dA, \tag{6}$$

where A_{gr} is the cross-sectional area of the groove, and the heat flux into the groove is given by

$$q''_{gr}(\vec{r},t) = -k_2 \left.\frac{\partial T_2}{\partial n}\right|_{\Gamma_2}, \tag{7}$$

which varies over Γ_2.

Eq. (6) must be solved at every instant in time until the vapor groove clears; the axial length of vapor in the groove, $z_g(t)$, is determined by integrating this rate relative to time. The solution is complicated by the fact that $z_g(t)$ is both time-dependent and also not known *a priori*. This makes it necessary to solve the transient, 3D problem using numerical methods in which the bubble growth rate and boundary length are determined by marching the solution forward in time. This solution scheme provides a rigorous means to determining evaporative heat transfer rates; this type of scheme has been quite successful at predicting experimentally measured growth rates in the nucleate boiling literature [17–19].

To obtain mathematical closure for the vapor growth model, the boundary condition at the outer radius of the evaporator's metal wall must be specified, and an initial condition must be specified for both the temperature profile in the evaporator and initial length of the vapor bubble. The boundary condition for the outer radius depends on the specific implementation of the CPL. When testing a CPL, a foil heater with relatively small thermal mass is typically wrapped around the evaporator. In this case, a boundary condition corresponding to a constant applied heat flux would be appropriate. On the other hand, if a large thermal mass (such as a metal flange and circuit board, as shown in Fig. 1) is conductively coupled to the evaporator and this mass is itself superheated, the model must include the added thermal mass as part of the solution domain.

The initial temperature profile of the evaporator depends on the preheating stage before nucleation occurs [2]:

$$T_i(\vec{r}, t=0) = f_i(\vec{r}), \tag{8}$$

where $f_i(\vec{r})$ is a specified function. For startups where a large thermal mass is attached to the evaporator and/or low powers are applied during the preheating stage, the temperature profile will be very nearly isothermal across the evaporator. Such a startup is the most stressing scenario since it represents the condition of greatest energy supply rate for a given wall superheat, and the lack of subcooling in the evaporator's core will cause any bubbles that may flow into the wick to grow.

The next parameter required for mathematical closure of the model is initial bubble length. When an embryonic bubble nucleates, its initial size is determined by the cavity from which it nucleates, which is very small compared to the length scales of the evaporator. Initial growth of the bubble diameter to the dimensions of the groove is extremely fast, and therefore neglected in the present model. Instead, the model assumes the vapor has already filled the groove's cross-section and specifies an initial axial length, L_0, of vapor equal to the groove's hydraulic diameter, $D_h = 4A_{gr}/P_{gr}$:

$$z_g(t=0) = L_0. \tag{9}$$

One final consideration in the bubble growth model is axial location of the first bubble along the groove. While nucleation is equally likely to occur at any axial location, the most stressing condition corresponds to nucleation at the evaporator end farthest from the vapor outlet. This condition would enable the accelerating vapor growth to traverse the full length of the evaporator, allowing for the largest possible pressure spike.

2.4. Simplified model

While the 3D model should accurately predict the vapor growth, its does not provide functional dependencies of the vapor growth on the evaporator's design parameters without examining numerical predictions for a large matrix of these parameters.

To better understand the effects of key design parameters, a simplified analytical model is also developed. The key simplifying assumption in this model is that heat conduction across the wick–groove interface is dominated by transient one-dimensional conduction from the wick–superheated liquid, as illustrated in Fig. 6. In other words, the heat flux is assumed uniform over the wetted perimeter P_w of the groove, and the rate of heat flow to the wick–groove boundary is time-dependent, but varies only in the axial direction. The simplified model also neglects axial conduction in the metal walls during the short transient associated with clearing of the first groove.

For one-dimensional transient conduction in a semi-infinite medium at a uniform initial temperature, the surface heat flux resulting from a step change ΔT in the surface temperature at time $t = 0$ is given by

$$q''_s(t) = \frac{k\Delta T}{\sqrt{\pi \alpha t}}. \tag{10}$$

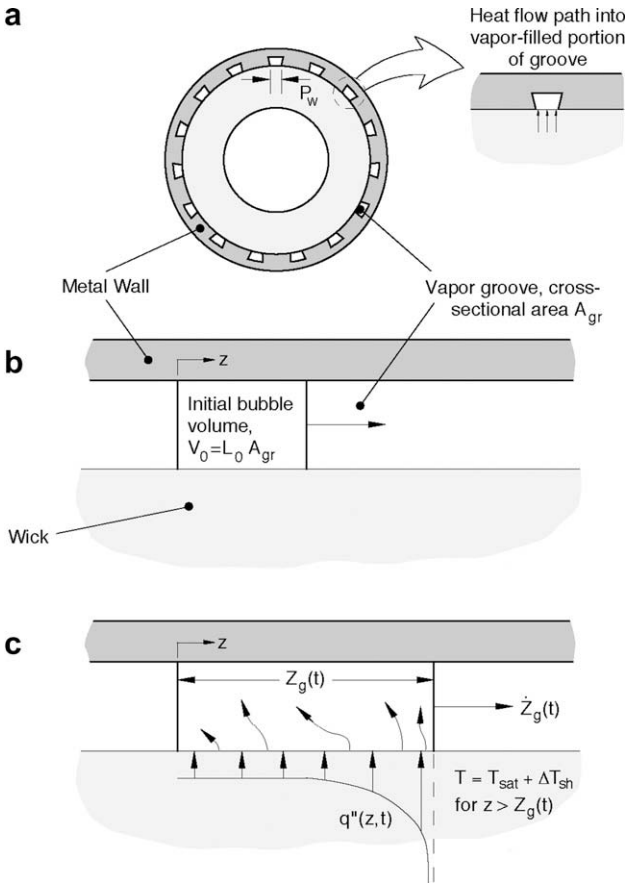

Fig. 6. Schematic illustrating assumptions and geometry used in simplified analytical bubble growth model. (a) Evaporator cross-section. (b) Axial section of vapor groove at $t = 0$. (c) Axial section at for $t > 0$. Because of assumed transient 1D conduction, transient heat flux varies only axially.

It is assumed that once the vapor–liquid front passes over an axial location z_0, the wick–groove boundary becomes exposed to saturated vapor, inducing transient conduction in the initially superheated wick in a direction perpendicular to the boundary. The resulting transient heat flux at z_0 is given by

$$q''(z_0,t) = \frac{k_2 \Delta T_{sh}}{\sqrt{\pi \alpha_2 (t - t_0)}}, \tag{11a}$$

where $$t_0 = Z_g^{-1}(z_0), \tag{11b}$$

which is the time at which the vapor–liquid front passes over location z_0, and k_2 and α_2 are, respectively, the thermal conductivity and diffusivity of the liquid-saturated wick; ΔT_{sh} is the wick's initial superheat.

The instantaneous volumetric rate of vapor generation is obtained from an energy balance written over the portion of the groove's length occupied by the vapor:

$$\dot{V}_g(t) = A_{gr}\dot{Z}_g(t) = \int_{z_0=L_0}^{Z_g(t)} P_w \frac{q''(z_0,t)}{\rho_g h_{fg}} dz_0 + L_0 P_w \frac{k_2 \Delta T_{sh}}{\rho_g h_{fg}\sqrt{\pi \alpha_2 t}}. \tag{12}$$

Substituting Eqs. (11a) and (11b) into (12) yields

$$\dot{Z}_g(t) = c \int_{z_0=L_0}^{Z_g(t)} \frac{dz_0}{\sqrt{t - Z_g^{-1}(z_0)}} + \frac{cL_0}{\sqrt{t}}, \tag{13a}$$

where $$c = \frac{k_2 \Delta T_{sh}}{\rho_g h_{fg}\sqrt{\pi \alpha_2}} \frac{P_w}{A_{gr}}. \tag{13b}$$

Using the identity relation

$$\frac{df^{-1}}{dx}(x) = \left[\left(\frac{df}{dy}\right)_{y=f^{-1}(x)}\right]^{-1}. \tag{14}$$

Eq. (13b) can be simplified to remove the inverse function from the integral, and is substituted into Eq. (13a) to yield

$$\dot{Z}_g(t) = c \int_{\tau=0}^{t} \frac{\dot{Z}_g(\tau)}{\sqrt{t - \tau}} d\tau + \frac{cL_0}{\sqrt{t}}. \tag{15}$$

Using LaPlace transforms [20], the length, $Z_g(t)$, of vapor in the groove becomes

$$Z_g(t) = L_0 \exp(\pi c^2 t)\left[1 + \mathrm{erf}\left(\sqrt{\pi c^2 t}\right)\right]. \tag{16}$$

3. Results

The mathematical 3D model is solved numerically using the finite volume technique [21] to determine vapor growth in the first groove to incur nucleation in a CPL evaporator. A Fortran code was developed in which the computational domain includes a heater plate (to simulate a circuit board) and a flange that conductively couples the heater plate to the evaporator. The code was validated, and appropriate mesh size and time step determined, when close agreement was reached between the model predictions and transient 3D benchmark configurations for which analytical solutions exist. Further refinements of mesh size and time step were exercised to ensure convergence of the evaporator-specific solution.

The presence of a large thermal mass leads to small temperature gradients across the evaporator at the end of the preheating stage. This results in a nearly uniform initial superheat in the evaporator at the onset of vapor generation, corresponding to the greatest pressure spike. In order to consider the most stressing scenario, the initial temperature is assumed uniform everywhere at $T_{sat} + \Delta T_{sh}$. The influence of ΔT_{sh} is examined parametrically.

A "baseline" evaporator design case is considered for the numerical simulations using ammonia as working fluid; Table 1 provides the key design parameters. These parameters correspond to an evaporator design for which experimental data were obtained during fully flooded startup. A superheat level of $\Delta T_{sh} = 3.9$ °C is used as baseline superheat, and saturation temperature is set at 35 °C. All material properties, except for those of vapor in the groove, are evaluated at this temperature and assumed constant since property variations are negligible over the range of temperature under consideration. Vapor in the groove is assumed saturated and its properties are evaluated at the pressure in the groove. For a startup to be successful, the differential pressure across the wick should not greatly exceed the maximum capillary pressure. Therefore, if the absolute pressure of the liquid core remains constant, the vapor properties in the groove should vary by less than 1%. Parameters for all numerical simulations presented below use baseline values with the exception of a single parameter that is varied in order to evaluate its effect on the vapor growth.

Fig. 7 shows vapor growth is strongly influenced by the initial superheat. Since the superheat provides the driving potential for heat transfer at the wick–groove interface, it is expected that increasing the initial superheat should increase the vapor growth

Table 1
Parameters of baseline evaporator design used in numerical model

Wall material	Stainless steel 304L
Wick material	Nickel (65% porosity)
Axial groove's cross-sectional area	0.72 mm^2
Axial groove's wetted perimeter	3.2 mm
Active length	0.371 m

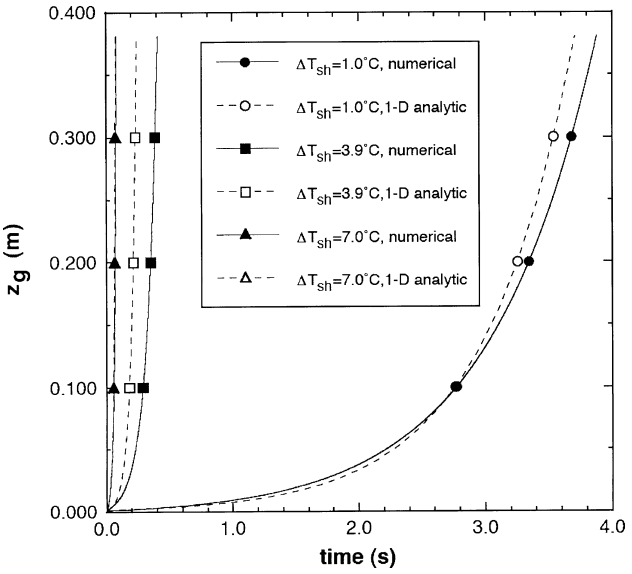

Fig. 7. Three-dimensional model and simplified analytical model predictions of the effects of initial superheat on vapor growth for base evaporator case.

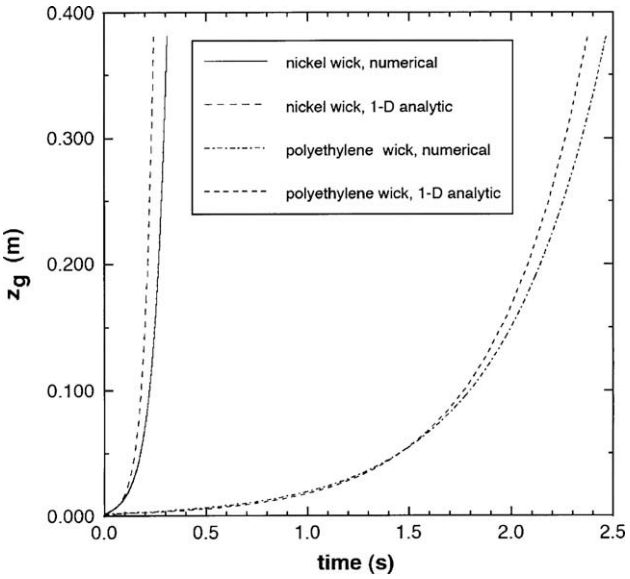

Fig. 9. Three-dimensional model and simplified analytical model predictions of the effects of wick material on vapor growth for 3.9 °C initial superheat.

rate, however, the predicted magnitude of change is quite dramatic. Fig. 7 shows increasing the superheat from 1 to 3.9 °C decreases the time to clear the groove by a factor of 10, and from 3.9 to 7.0 °C by an additional factor of 4. Results from the simplified analytical model, which are also included in Fig. 7, are in excellent agreement with the 3D predictions for the 1.0 and 7.0 °C superheats, with the 3.9 °C superheat producing the greatest departure – as much as 50%. Nonetheless, these results demonstrate the effectiveness of the simplified model at predicting both the trends and the profound effects of initial superheat on vapor growth.

By examining Eq. (16), it is apparent that the growth rate can be reduced substantially by reducing the magnitude of c, given by Eq. (13b). Fig. 8 shows how increasing the groove's cross-sectional area, A_{gr}, (in order to decrease c) is a very effective means for reducing the vapor growth rate. Fig. 8 also shows the simplified analytical model is quite effective at capturing the influence of A_{gr} on the vapor growth. A similar trend is achieved (but not shown here) by *decreasing*the wetted perimeter, P_W.

The effects of wick material are presented in Fig. 9. Using a low conductivity polyethylene wick instead of a nickel wick (in order to decrease c) is shown greatly slowing the vapor growth rate. This effect is as profound as that of the groove's cross-sectional area or wetted perimeter. Fig. 9 also proves that the simplified analytical model is fairly effective at capturing the influence of wick material.

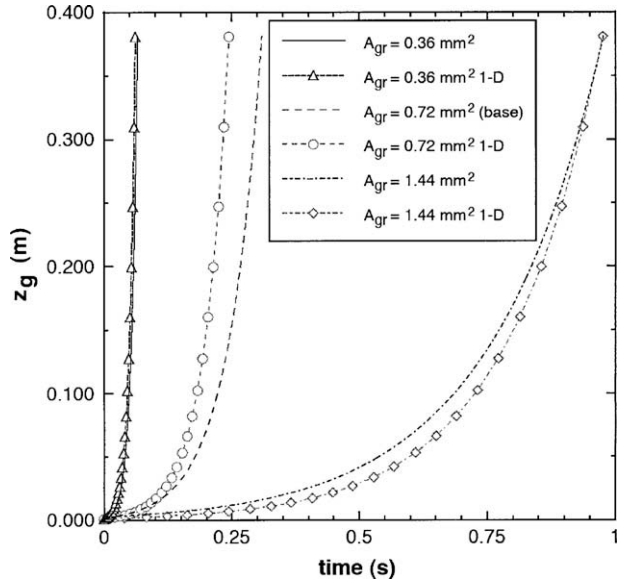

Fig. 8. Three-dimensional model and simplified analytical model predictions of the effects of the groove's cross-sectional area on vapor growth.

4. Conclusions and recommendations

Early vapor growth in the evaporator of a CPL is responsible for liquid acceleration that results in a differential pressure spike. A large pressure spike can deprime the evaporator by forcing vapor into the evaporator's wick, which is the only failure mode of a CPL other than fluid loss or physical damage to the loop. A 3D transient conduction model is constructed to predict vapor growth in the first groove of the evaporator to nucleate. This model is used to examine the influence of key design parameters on the vapor growth. A simplified model is also presented which facilitates the assessment of parametric influences by analytic means. Key findings from the study are as follows:

(1) Predictions of the time required to clear the first groove using the analytical model vary by as much as 50% from those of the 3D numerical model. While the predictive differences for certain cases are by no means small, the simplified model is highly effective at capturing the influences of individual design parameters.
(2) The evaporator's initial superheat has the most significant influence on vapor growth rate. Decreasing the superheat from 7 to 1 °C increases the clearing time from less than 0.1 to 3.9 s.
(3) The growth rate can also be greatly decreased by increasing the groove's cross-sectional area, A_{gr}, or decreasing the wetted perimeter, P_W, or by simply minimizing the ratio P_W/A_{gr}. This can be accomplished by using trapezoidal grooves in the evaporator's metal wall that are both deep and steep-angled. On the other hand, machining grooves directly into the wick increases P_w/A_{gr} appreciably, resulting in adverse vapor growth effects.

(4) The vapor growth rate may be slowed appreciably by using low conductivity wick material such as polyethylene instead of metal.

References

[1] I. Mudawar, Assessment of high-heat-flux thermal management schemes, IEEE Trans. CPMT: Comp. Pack. Tech. 24 (2001) 122–141.
[2] T.J. LaClair, I. Mudawar, Thermal transients in a capillary evaporator prior to the initiation of boiling, Int. J. Heat Mass Transfer 43 (2000) 3937–3952.
[3] J. Ku, Overview of capillary pumped loop technology, in: Proceedings of the 29th National Heat Transfer Conference, HTD, vol. 236, Atlanta, GA, 1993, pp. 1–17.
[4] B.A. Cullimore, Capillary pumped loop application guide, SAE Paper 932156, Warrendale, PA, 1993.
[5] B.A. Cullimore, Start up transients in capillary pumped loops, AIAA Paper 91-1374, Reston, VA, 1991.
[6] D. Antoniuk, J. Pohner, Deleterious effects on non-condensible gas during capillary pumped loop startup, SAE Paper 941408, Warrendale, PA, 1994.
[7] D. Antoniuk, D.K. Edwards, Depriming of arterial heat pipes: an investigation of CTS thermal excursions, Final Report, NASA CR 165153, TRW Report 34129-6001-UT-00, Washington, DC, 1980.
[8] W.M. Rohsenow, Boiling, in: W.M. Rohsenow, J.P. Hartnett (Eds.), Handbook of Heat Transfer, McGraw-Hill, New York, NY, 1973.
[9] D. Butler, L. Ottenstein, J. Ku, Flight testing of the capillary pumped loop flight experiment, SAE Paper 951566, Warrendale, PA, 1995.
[10] D. Antoniuk, An investigation of the CAPL flight experiment thermal anomalies, SAE Paper 951717, Warrendale, PA, 1995.
[11] L. Ottenstein, J. Nienberg, Flight testing of the two-phase flow flight experiment, SAE Paper 981816, Warrendale, PA, 1998.
[12] D. Antoniuk, J. Nienberg, Analysis of salient events from the two-phase flow (TPF) thermal control flight experiment, SAE Paper 981817, Warrendale, PA, 1998.
[13] S.R. Clayton, D. Martin, J. Baumann, Mars surveyor thermal management using a fixed conductance capillary pumped loop, SAE Paper 972467, Warrendale, PA, 1997.
[14] W. Qu, I. Mudawar, Flow boiling heat transfer in two-phase micro-channel heat sinks. II. Annular two-phase flow model, Int. J. Heat Mass Transfer 46 (2003) 2773–2784.
[15] W. Qu, S.-M. Yoon, I. Mudawar, Two-phase flow and heat transfer in rectangular micro-channels, ASME J. Electron. Pack. 126 (2004) 288–300.
[16] D.A. Nield, A. Bejan, Convection in Porous Media, Springer-Verlag, New York, NY, 1992.
[17] M.S. Plesset, S.A. Zwick, The growth of vapor bubbles in superheated liquids, J. Appl. Phys. 25 (1954) 493–500.
[18] H.K. Forster, N. Zuber, Growth of a vapor bubble in a superheated liquid, J. Appl. Phys. 25 (1954) 474–478.
[19] L.E. Scriven, On the dynamics of phase growth, Chem. Eng. Sci. 10 (1959) 1–13.
[20] M.N. Özisik, Heat Conduction, John Wiley and Sons, New York, NY, 1980.
[21] S.V. Patankar, Numerical heat transfer and fluid flow, Hemisphere Publishing Corp., New York, NY, 1979.